



Numerical Identification of Flow-Induced Oscillation Modes in Rectangular Cavities using URANS

M. Mesbah[†] and S. Majidi

Faculty of Mechanical and Energy Engineering, Shahid Beheshti University, Tehran, Iran

[†] Corresponding Author Email: m_mesbah@sbu.ac.ir

(Received February 16, 2019; accepted July 13, 2019)

ABSTRACT

The present research focuses on flow oscillations in a planar rectangular cavity. The compressible URANS equations in combination with transition SST $k-\omega$ model are utilized to include the turbulence effects. The simulations are carried out for low Reynolds flow with Mach number ranging from 0.2 to 0.7. Flow features are investigated and the frequency analysis is discussed. Two flow oscillation modes, namely shear-layer mode and wake mode are thoroughly identified. The flow structure and oscillation frequencies compare well with LES and DNS results presented in the literature. Furthermore, the shear mode frequency is well aligned with that predicted by Rossiter. This research is aimed to evaluate the performance of URANS as an industrially attractive tool to capture flow phenomena, previously visualized by the aforementioned sophisticated methods.

Keywords: URANS; Cavity flow; Self induced oscillation; Shear-layer mode; Wake mode; Mode detection.

NOMENCLATURE

D	cavity depth	T	temperature
f	frequency	U	free stream velocity
M	Mach number	u_i	velocity component
K	kinetic energy	ν_t	turbulent viscosity
L	cavity length		
Re_D	Reynolds number defined based on cavity depth	θ_0	Momentum thickness
P	pressure	ρ	density
Pr_t	turbulent Prandtl number	τ_R	Reynolds stress
Str	Strouhall number		

1. INTRODUCTION

In industrial environments the dominant noise which is mainly generated by rotary machines is tonal noise. In addition to the industrial machines, the generated noise by most of household electrical devices such as hair dryer, vacuum cleaner, kitchen hood, ventilation fan, etc is characterized by the tonal noise. In the noise spectrum of any device which consists of a rotary part, a peak corresponding to the rotational speed or its higher harmonics can be detected. Not only rotary machines, also some flow devices with stationary parts like cavities deal with the tonal noise. Flow passing over a cavity can be seen on a broad range of devices. These include, but not limited to musical instruments, aircraft landing

gear and weapon bay, automotive industry, gas transport systems and aerospace applications. The spectrum of cavity noise contains both broadband components, introduced by the turbulence in the shear layer, and tonal components. Regarding the tonal component, two mechanisms are responsible: a wake mode mechanism where a periodic vortex shedding at the cavity leading edge takes place and a shear-layer mode mechanism where a feedback coupling between the flow field and the acoustic field occurs.

Due to its vast range of industrial applications, cavity flow oscillations, has been an interesting research topic for decades. Rossiter was among the pioneers who introduced an acoustic feedback mechanism (Rossiter, 1964). A shear layer, formed by flow,

amplifies disturbances which are subsequently scattered into acoustic waves at the trailing edge corner. These acoustic waves while propagating upstream excite disturbances in the shear layer resulting to creation of a feedback loop. This often leads to self-sustained oscillations with discrete resonant frequencies. He also proposed a semi-empirical formula to estimate the dimensionless oscillation frequencies (Strouhal number, Str):

$$Str = \frac{fL}{U_\infty} = \frac{n - \gamma}{M + 1/k}, \quad n = 1, 2, \dots \quad (1)$$

with f the frequency, L the length of the cavity, U_∞ the free-stream velocity, n the mode number, M the Mach number, and constants k and γ are 0.57 and 0.25, respectively.

Two distinct types of flow oscillations inside the cavity named as shear-layer mode and wake mode are revealed by Numerical and experimental studies. The shear layer mode oscillation is characterized by the aforementioned acoustic feedback. In the numerical simulations, as the Mach number, length to depth ratio, and Reynolds numbers are increased a substantial change in the flow inside the cavity is observed. Flow oscillation is evidently witnessed in the wake mode under these conditions. In this mode, the vortex generated at the cavity leading edge grows to nearly the size of the cavity. Subsequent collision between the wall and the large vortex forms a small vortex in between. This vortex forces the large vortex to be shed from the leading edge and a large eruption of vortical fluid leaves the cavity. The wake mode oscillation was initially observed via experiment in an axisymmetric cavity at very low speed (0.23 m/s) in an incompressible flow (water) (Gharib & Roshko 1987).

Hybrid methods have been developed as a practical approach in numerical study of aeroacoustics. In this methodology, flow field and acoustic equations are solved separately in their respective zones of the computational domain (Maillard & Bailly 2001; Gloerfelt, Bogey, & Bailly 2002). Various coupling techniques have been proposed to link the flow field governed by Navier-stokes equations and acoustic field governed by linearized Euler equations (LEE) (Mesbah, Meyers & Baelmans 2008; Ali, Becker, Utzmann & Munz 2008; Djambazov, Lai & Pericleous 2000). Although the flow field is a small portion of whole domain in the hybrid approach, the accuracy of the predicted far-field noise and also computational cost are determined by this part. Whether a tonal or a white noise is major interest, different methods can be employed to obtain the flow field solutions.

Regarding the white noise, a hybrid approach either based on Stochastic Noise Generation and Radiation (SNGR) or DNS and LES can be used. In SNGR method, the steady state behavior of flow field is estimated by a RANS solution (Mesbah, 2006). Next, a stochastic turbulence field based upon averaged values obtained from RANS is generated which is further used as the source of acoustic waves. Besides all uncertainties associated with SNGR methods, whether RANS solution as the base of this

method is an accurate representative for averaged flow behavior is still an open question. Concerning the DNS solution, so far its application is limited to only academic research. For example, Rowley (2002) studied two dimensional cavity flow oscillations using DNS where they detected both oscillating regimes. Respecting the LES-based hybrid approach, it should be noted that it is capable of capturing both tonal and white noises. Several academic researches using LES were conducted to capture flow instabilities responsible for self-sustained oscillations in the flow field. Chang *et al.* (2006) conducted a research on vortex structures demonstrated in incompressible flows passed over shallow cavities. Larchevêque *et al.* (2004) used LES to investigate the main mechanism responsible for production of self-sustained acoustic waves in subsonic cavity flows. De Roeck *et al.* (2009) compared capability of different coupling approaches in predicting the generated noise in compressible flows over two dimensional cavities. Large eddy simulation has also been used in studying noise generation in supersonic cavity flows (Nair and Sarkar, 2017; Wang, Sun, Qin, Wu, and Wang, 2013; Li, Nonomura, Oyama, and Fujii, 2012; Li, Nonomura, and Fujii, 2013). However, it should be pointed out that the practicability of these approaches are limited to academic case studies due to its computationally expensive numerical schemes.

On the subject of the tonal noise, in addition to the aforementioned methodologies, i.e. LES and DNS, solutions obtained using a low cost numerical scheme such as URANS computations are highly appreciated. In this context, a few researches have been conducted to study cavity flow oscillation and also cavity flow noise using RANS. Henderson used URANS to study the subsonic and transonic shallow cavity flow (Henderson, Badcock, and Richards, 2000) reporting a good agreement between experiments and simulations. Investigations upon two and three-dimensional open shallow cavity flows were conducted by Shieh and Morris (2001) for understanding noise characteristics. They used Spalart-Allmaras turbulence model in the vicinity of walls to avoid extra computational cost resulted by grid clustering. To remedy excessive dissipation of their RANS model, they employed LES computations in regions far from the walls. Sinha *et al.* (1998) examined application of two different RANS models (algebraic and two equation models) in their simulation of compressible flow over open cavities. However, they reported severe shortcomings of their RANS approach to model flows with non-resonant turbulence-acoustic coupling in comparison to their VLES results. Ahn *et al.* (2008) investigated aeroacoustics of flows over deep cavities using $k - \varepsilon$ turbulence model. However, acute suppression of flow oscillations were witnessed due to excessive turbulence viscosity of the model. Therefore, they adopted partially resolved numerical simulation (PRNS) technique introduced by Shih and Liu (2004) to overcome the above mentioned deficit. Kultu *et al.* (2015) applied a $k - \omega$ based numerical solver to study the effects of bottom injection on acoustical characteristics of flows over deep cavities. They focused on flows with a free-stream Mach number of

0.3 in cavities with depth to length ratio of 4.68. Thus, aeroacoustics of the wake mode regime were not investigated. URANS was used to assess noise radiation in low Mach number flows over cavities with neck and porous insert (Shao and Li, 2015; Ashcroft, Takeda, and Zhang 2003). Also, acoustic analogy employing porous Ffowcks Williams Hawking were used to predict far-field noise propagation. Their results, although promising for application in sound radiation control, were limited to a free stream Mach number of 0.15. Sun *et al.* (2017) investigated the stability attributes of two and three-dimensional cavities for a specific length to depth ratio at a free stream Mach number of 6. They used DNS along with bi-global analysis in their investigation on stability properties of wake mode. Lucas *et al.* (2017) studied the formation of wake modes in tubulrnt flow over Ahmet bodies with flat back and cavity in the backside. They investigated the pefomance of cavities with various depths in drag reduction. Sun *et al.* (2018) studied side wall effects on the properties of three dimensional cavity flows using LES. To the extent of authors knowledge, no comprehensive research has been conducted using URANS approach to study oscillatory flow regimes in a variety of freestream Mach numbers where URANS capabilities can be compared with more detailed approaches like LES and DNS. Therefore, the purpose of this study is to investigate the performance of steady and unsteady RANS as the bases of the acoustic hybrid methods to capture essential features of cavity flow.

In this research, 2D compressible URANS computations are carried out to reproduce and characterize the self-induced cavity flow oscillation regimes, i.e. shear-layer and wake modes. Flow turbulence is accounted for utilizing the transition SST $k - \omega$ turbulence model (Menter, Langtry, Likki, Suzen, Huang, and Völker, 2006). The flow features are discussed and the ability of URANS approach to capture the flow phenomena is evaluated by comparing the results with those of LES and DNS. It is worth noting that the wake mode has been perfectly visualized by LES and DNS methodology even for a compressible flow at a moderate Mach number. Nonetheless, the applications of these approaches to complex geometries is limited and their computational cost is still prohibitive for high Reynolds number flows. Thus, the hybrid methodology based on steady and unsteady RANS presents a promising perspective in dealing with noise prediction problems occurring in industrial applications.

The paper is organized as follows. First, the computational setup is illustrated. Then, the flow features obtained from URANS simulations are discussed. Next, frequencies of flow oscillations are analyzed and compared with results obtained by other approaches. At the end, a summary of the work is presented and some conclusions are drawn.

2. COMPUTATIONAL SETUP

The unsteady Reynolds Averaged Navier-Stokes

equations are considered as the set of governing equations and can be written in tensor form as:

$$\frac{\partial \rho}{\partial t} + \frac{\partial \rho u_i}{\partial x_i} = 0 \quad (2)$$

$$\frac{\partial \rho u_i}{\partial x_i} + \frac{\partial \rho u_i u_j}{\partial x_j} = - \frac{\partial P}{\partial x_i} + \frac{\partial \left[\mu \left(\frac{\partial u_i}{\partial x_j} + \frac{\partial u_j}{\partial x_i} - \frac{2}{3} \delta_{ij} \frac{\partial u_l}{\partial x_l} \right) + \tau_{R,ij} \right]}{\partial x_j} \quad (3)$$

$$\frac{\partial \rho (e + 0.5(u_i u_i))}{\partial t} + \frac{u_i (\partial \rho (e + 0.5(u_i u_i)) + P)}{\partial x_i} = \frac{\partial \left[u_i \left(u \left(\frac{\partial u_i}{\partial x_j} + \frac{\partial u_j}{\partial x_i} - \frac{2}{3} \delta_{ij} \frac{\partial u_l}{\partial x_l} \right) + \tau_{R,ij} \right) \right]}{\partial x_j} + \frac{\partial \left[\left(k + \frac{c_P \rho v_t}{Pr_t} \right) \left(\frac{\partial T}{\partial x_i} \right) \right]}{\partial x_i} \quad (4)$$

In the above set of equations, ρ , P , u_i , and T represent averaged values for density, pressure, velocity component, and temperature. Also, k , v_t , and Pr_t indicate turbulent kinetic energy, turbulent kinematic viscosity, and turbulent Prandtl number. Symbol $\tau_{R,ij}$ represents Reynolds stress defined as:

$$\tau_{R,ij} = \rho v_t \left(\frac{\partial u_i}{\partial x_j} + \frac{\partial u_j}{\partial x_i} - \frac{2}{3} \delta_{ij} \frac{\partial u_l}{\partial x_l} \right) - \frac{2}{3} \rho k \delta_{ij} \quad (5)$$

Transition SST $k - \omega$ model proposed by Menter *et al.* (2006) is used to obtain Reynolds stress components. Simulations are performed on a two-dimensional rectangular cavity using finite volume based flow solver. In this model the reynolds stresses are calculated using an eddy diffusivity approach where turbulent viscosity is obtained as follows.

$$v_t = \min \left(\frac{\rho k}{\omega}, \frac{a_1 \rho k}{S F_2} \right) \quad (6)$$

In this equation, k and ω represent turbulent kinetic energy and specific dissipation rate respectively. Also, S indicates strain rate and F_2 is computed as a function of k , ω , and distance from the nearest surface. k and ω are obtained via the following transport equations.

$$\frac{\partial (\rho k)}{\partial t} + \frac{\partial (\rho u_i k)}{\partial x_i} = \tilde{P}_k - \tilde{D}_k + \frac{\partial \left((\mu + \sigma \mu_t) \frac{\partial k}{\partial x_i} \right)}{\partial x_i} \quad (7)$$

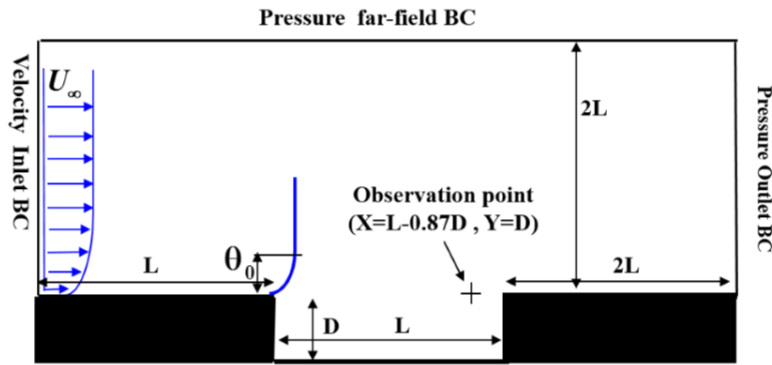


Fig. 1. Sketch of the computational domain.

$$\frac{\partial(\rho\omega)}{\partial t} + \frac{\partial(\rho u_i \omega)}{\partial x_i} = \frac{\alpha P_k}{\nu_t} - D_\omega + C d_\omega + \frac{\partial\left((\mu + \sigma\mu_t) \frac{\partial\omega}{\partial x_i}\right)}{\partial x_i} \quad (8)$$

$$\begin{aligned} \tilde{P}_k &= \gamma_{eff} * P_k \\ \tilde{D}_k &= \min(\max(\gamma_{eff}, 0.1), 1.0) D_k \end{aligned} \quad (9)$$

The terms P_i and D_i represent the production and destruction rates of variable i . Also, γ_{eff} is the effective intermittency which is determined based on separation intermittency in transition from laminar to turbulent flow.

The set of governing equations are numerically solved in the computational domain shown in Fig. 1 utilizing the coupled algorithm. The cavity has the length to depth ratio (L/D) of 4 and simulations are performed for Mach numbers ranging from 0.2 to 0.7. The computational domain extends respectively one and two times the cavity length in upstream wise from the cavity leading edge and downstream wise from the cavity trailing edge. Also, the extending length in the upward direction is two times the cavity length. Spatial derivatives are approximated using second order discretization schemes in momentum and continuity equations. To increase stability of the numerical algorithm, gradients present in the energy equation and the turbulence model are discretized with first order accuracy. Second order implicit discretization scheme is used to perform time integration. Time-step sizes are chosen so that typical oscillation periods in each computational case consist of at least 45 time steps. The Reynolds number based on cavity depth (Re_D) is 1500 in all cases. The setup is similar to the numerical setup presented in references (Rubio, De Roeck, Baelmans, and Desmet, 2007; Rowley, 2002), where LES and DNS simulations are performed respectively. It should be mentioned that the imposed initial conditions of each transient case is obtained from the converged solution of its RANS counterpart. Thus, the inlet velocity profile prescribed in the RANS simulation is determined in a way that L/θ_0 reaches its predetermined value of 102. The parameter θ_0 corresponds to the momentum

thickness of the boundary layer at the upstream edge in RANS solution. Inlet velocity is calculated based on Blasius self-similar solution for flow over a flat plate.

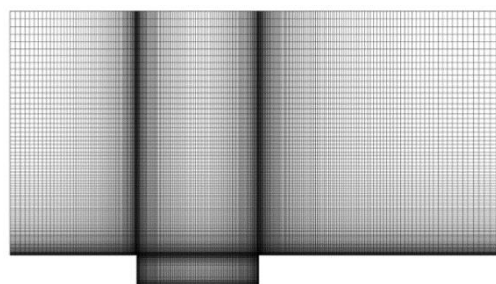
Furthermore, the URANS simulations are performed using the simplistic Cartesian multi-block grid. Figure 2 shows grid blocks as well as the details of the generated grid around the leading edge of the cavity. The grid is clustered around the edges in order to provide a better resolution of flow gradients. The computational domain is decomposed into two mesh blocks covering the cavity and the sub-domain above the cavity. The cavity block consists of 120×50 mesh points and the upper block has 310×100 mesh points. The mesh is sufficiently refined in near wall regions in a way that $Y^+ \leq 1$ for all wall sided cells in the entire domain. Thus, viscous sub layer is resolved and there is no need to use wall function. In order to assess independence of the obtained results from mesh spacing or boundary positions, the simulations are repeated using finer mesh spacing with larger domain extensions. The obtained results did not indicate any noticeable difference from those of the present computational setup in terms of frequency and amplitude of vortex shedding. Thus, results presented in this paper are confirmed to be mesh independent.

3. FLOW FEATURES

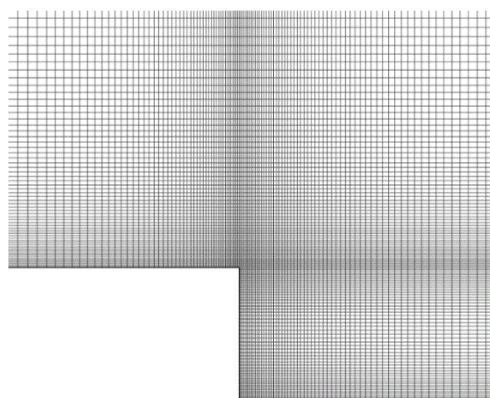
In order to study the physical structure of flow inside the cavity, both steady and unsteady RANS calculations are used for various inlet flow Mach numbers ranging from 0.2 to 0.7. Figures 3(a) and (b) illustrate the flow streamlines inside of cavity for the inlet Mach number of 0.3 and 0.6, respectively. It can be seen that in both cases two dominant vortices occupy the cavity and show almost the same patterns. The large one spread along the whole cavity with the center near the downstream wall. Collision between the wall and the dominant vortex forms a contrarotative vortex. This vortex which is located near the bottom of cavity causes a flow blockage and forces the large vortex to be split. For the case $M=0.3$ in which the shear layer has less energy, a small vortex can be seen inside the large one.

Flow fields obtained from unsteady RANS

simulations present different flow features inside the cavity than those obtained from steady RANS. Energy transfer from flow passing above the cavity through the shear layer makes it unstable. Further development of the instabilities leads to an oscillatory flow. The obtained results reveal two regimes of oscillations: shear layer mode and wake mode. In the shear layer mode the acoustic feedback coupling, explained in the introduction section, governs the flow oscillation. Figure 4 shows vorticity and pressure contours for the case $M=0.3$ as the indicative of shear layer oscillation mode. The figure presents the contours at three different instants, corresponding to approximately one-third phase intervals of the second Rossiter mode, which is dominant for this computation. It can be seen from vorticity contours that the shear layer bridges the cavity with harmonic oscillations in the mouth of cavity. Generally when the cavity is deep enough, a steady vortex is trapped at the rear half of the cavity with a small deformation. For the current test case, the trapped vortex violently deformed during one cycle of oscillation. Evidently, the interaction of the shear layer with the flow inside the cavity is not weak enough to sustain the shear-layer mode and the flow has tendency to switch to wake mode. Figure 4 also presents the pressure contours which indicates the regions with relative negative and positive pressure values. The regions with negative values coincide the core of vortices and the positive values illustrate the regions where the collision of two vortices or vortex-solid walls occur.

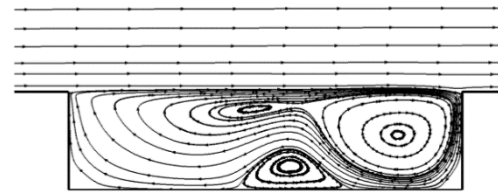


(a) Multi-block Grids

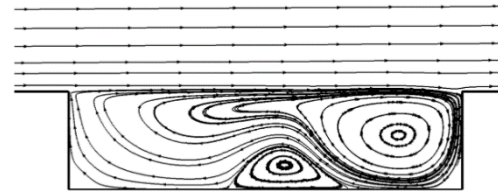


(b) Grid refinement around the leading edge

Fig. 2. Generated Mesh.



(a) $M=0.3$



(b) $M=0.6$

Fig. 3. Mean flow streamlines inside the cavity obtained from steady RANS.

As mentioned previously in this paper, increasing the length to depth ratio of cavity, Mach and Reynolds numbers lead to a substantial change in the oscillation manner by switching it to the wake mode. In this study, only increasing the Mach number from 0.3 to 0.4 while maintaining the rest of parameters constant, i.e. cavity length-to-depth ratio ($L/D=4$), cavity length-to-momentum thickness ratio ($L/\theta_0=102$) and the Reynolds number ($Re_D = 1500$), transition between the shear layer mode to wake mode takes place. The wake mode is characterized by a large scale vortex shedding from the cavity leading edge. The vortex formed at the leading edge of the cavity grows until nearly the size of cavity. Further collision between the wall and the large vortex generates a small vortex in between. This vortex forces the large vortex to be shed from the leading edge and a large eruption of vortical fluid leaves the cavity. Figure 5 shows the sequences of vortex shedding for the case $M=0.6$. Vorticity and pressure contours are presented at five different instants, corresponding to one-fifth time intervals of an eruption period. It can be seen that the upstream boundary layer experiences a separation with the growth of the dominant vortex. Also downstream boundary layer is dramatically affected by vortex removal. The regions with relative negative pressure, as previously mentioned is coincident with the vortex core. Moreover, the negative pressure in the first half of the cavity is due to the evacuation of the large vortex which is convected away by the mean flow.

To further investigate the flow feature of the cavity, a time average over 4 periods of oscillations is performed during the URANS computations. Figures 6(a) and (b) show the time-averaged streamlines for the case $M=0.3$ (shear-layer mode) and $M=0.6$ (wake mode), respectively. It can be observed that in the wake mode, the size of dominant vortex equals the length of cavity so that the streamlines above the cavity are clearly deflected. In comparison with DNS solution (Rowley, 2002), the presented flow patterns for the wake mode are similar and only a small difference at the location of the vortex center can be observed. In URANS solution the center of vortex is at the middle of cavity ($x=L/2$) while in DNS it is

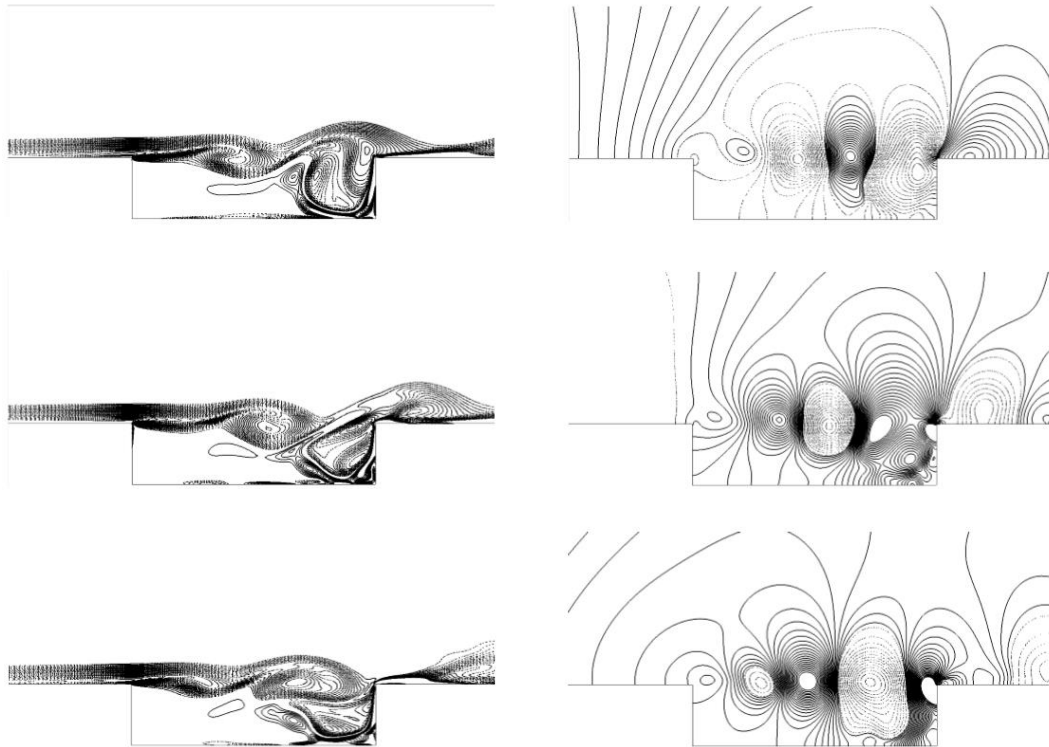


Fig. 4. Flow oscillation with the shear-layer mode inside the cavity for $M=0.3$. On the left: vorticity field during one cycle of oscillation. 26 contours of $\frac{\omega D}{U}$ are shown between -5 and 3. On the right: Pressure fluctuation contours at the same instants. 50 contours of $\frac{p-p_\infty}{\rho U_\infty^2}$ are shown between -0.7 and 0.7. Negative contours are dashed in both cases.

slightly towards the upstream, roughly 10%. Regarding the shear layer mode, the flow structures are nearly similar to the reported ones (Shieh and Morris, 2001; Rubio, De Roeck, Baelmans, and Desmet, 2007; Rowley, 2002) for this type of oscillation consisting of two vortices, one at the rear up and another one down front and also the mean flow streamlines above the cavity are nearly horizontal along the mouth of the cavity.

Another interesting comparison can be made is between the RANS and time-averaged URANS solutions, as presented in Fig. 3 and Fig. 6. It can be seen that the flow patterns for both cases drastically change. Furthermore, a comparison between the velocity profiles may provide a better insight to the flow features. Figure 7 compares the velocity profiles at different sections. For the case $M=0.3$ (shear-layer mode) only the flow field in the rear half of the cavity is significantly modified from the RANS solution. For $M=0.6$, wake mode oscillations not only have a significant impact on the mean flow inside the cavity but also outside the cavity. The affected zone above cavity has a spreading radius equal to the cavity depth. It is important to remark that the wake mode oscillations influence the structure of the mean flow even in the upstream direction. Thus, the momentum thicknesses at the leading edge, measured through the RANS calculations, are substantially different from those that are found in the time averaged URANS computations. It can be concluded from the

comparison between RANS and URANS that the steady RANS solutions might mislead the researchers. It means the effects of unsteadiness in cavity flow should not be ignored.

Table 1 Overview of flow oscillation modes using different approaches

	DNS	LES	URANS
$M=0.2$	shear layer	shear-layer	shear-layer
$M=0.3$	mixed	mixed	shear-layer
$M=0.4$	wake	mixed	wake
$M=0.5$	wake	wake	wake
$M=0.6$	wake	wake	wake
$M=0.7$	wake	not available	wake

An overview of the oscillation modes that are obtained using different approaches is presented in Table 1. For the case $M=0.2$ all approaches, i.e. DNS, LES and URANS identify the shear-layer mode. In the case $M=0.3$, the mixed mode is detected by DNS and LES solutions while URANS predicts the shear-layer mode. This is due to inability of URANS to resolve eddies in inertial subrange and the lower scales. Thus, the onset of transition from shear-layer to wake mode is delayed relative to DNS and LES solutions. It can be expected since URANS is known to be dissipative of small disturbances which trigger flow instabilities. By increasing the free stream

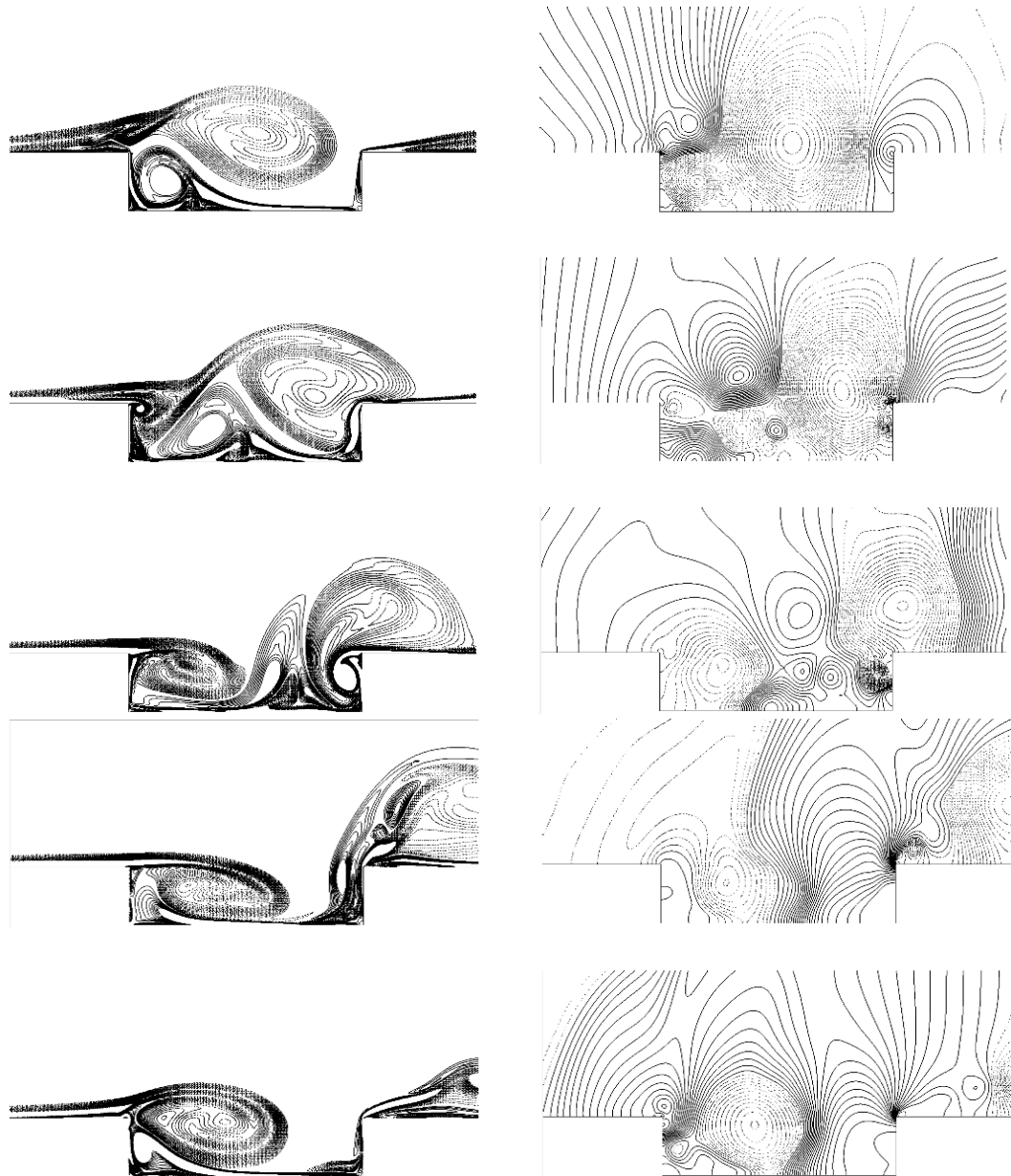
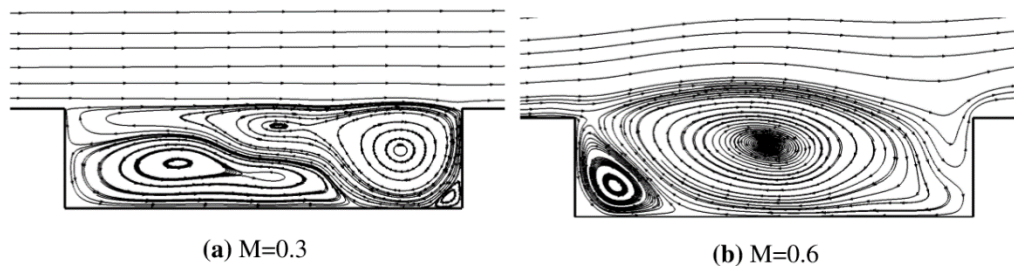


Fig. 5. Flow oscillation with the wake mode inside the cavity for $M=0.6$. On the left: vorticity field during one cycle of oscillation. 26 contours of $\frac{\omega D}{U}$ are shown between -5 and 3. On the right: Pressure fluctuation contours at the same instants. 50 contours of $\frac{p-p^\infty}{\rho U_\infty^2}$ are shown between -0.7 and 0.7. Negative contours are dashed in both cases.



(a) $M=0.3$ (b) $M=0.6$
Fig. 6. Mean flow streamlines inside the cavity obtained from Unsteady RANS.

Mach number to 0.4, URANS as well as DNS reveal a full transition but LES captured the mixed mode.

For higher Mach number, all approaches detect the wake mode.

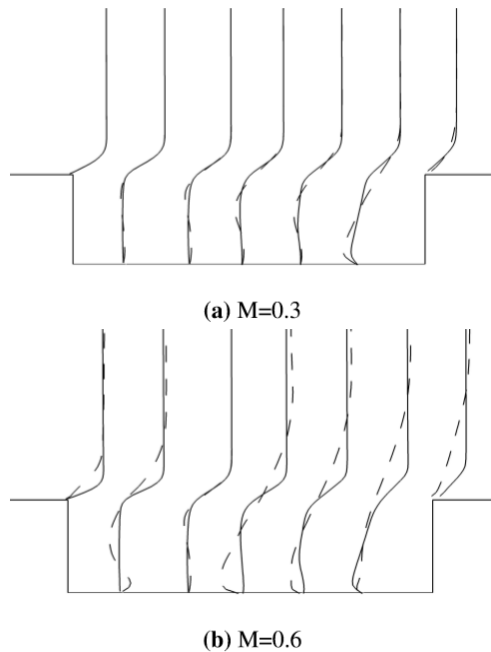


Fig. 7. Comparison of mean velocity flow profile inside the cavity obtained from Steady RANS and URANS. Dashed line indicates URANS solution, while the solid line indicates the RANS solution.

4. FREQUENCY ANALYSIS OF OSCILLATIONS

For each simulation, the time signals of primitive variables are recorded at the observation point which is located at the mouth of cavity at $X = L - 0.87D$ (shown in Fig. 1). Here, only the data which have been recorded after converging to a steady periodic oscillation are presented and used. In the spectrum of every case, at least a distinct tonal peak and its harmonics become evident.

Time trace of pressure signal for an interval of 1.6×10^{-5} seconds at the observation point for different Mach numbers are shown in Fig. 8. The relative amplitude of oscillations has been kept unmodified for comparison. A quick glimpse to the figure reveals that the oscillations for all cases are periodic and no switching between the modes exist. Considering the fact that the URANS computations inherently damp the small disturbances, having a clean periodic signal in comparison with the ones obtained from LES (Rubio, De Roeck, Baelmans, and Desmet, 2007) and DNS (Rowley, 2002) is expected. In Fig. 8 the amplitude of oscillation for case $M=0.2$ is almost not visible since it is very small in comparison with the other cases. By increasing the inlet flow velocity the oscillations are magnified but the amplification from the case $M=0.3$ to $M=0.4$ is noticeable. This is caused by the fact that the transition from shear-layer mode to the wake mode happens in between. Moreover, it should be noted that by increasing the Mach number in each oscillatory modes the frequency of fluctuations increases.

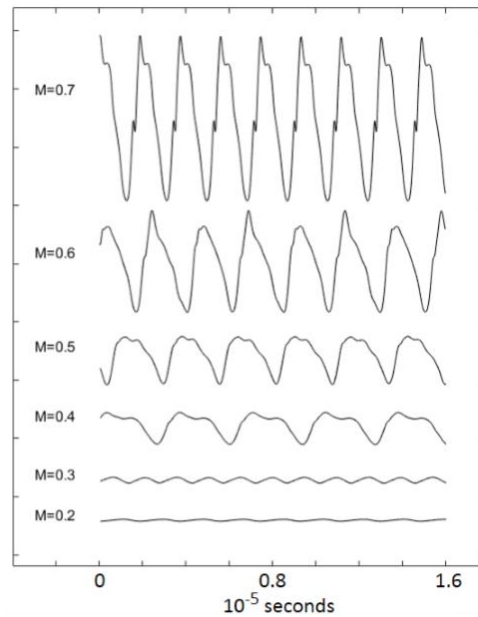
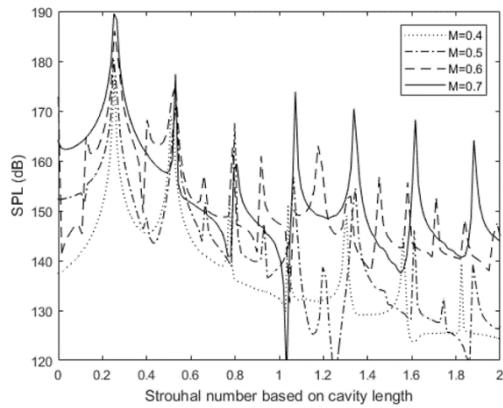


Fig. 8. Time trace of pressure signal for different Mach numbers after converging to a steady periodic oscillation.

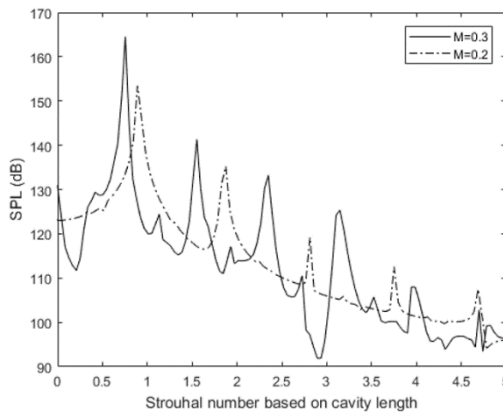
A Fourier analysis of the recorded pressure signals provides the frequency spectrum which confirms the identification of the oscillation modes presented in Table 1. Figure 9 shows the calculated spectrum where the vertical axis is in terms of Sound Pressure Level (dB) and the horizontal axis is in terms of dimensionless frequency (Strouhal number). The spectrum of cases which oscillate in shear-layer mode are presented in Fig. 9(a). Increasing the Mach number by 0.1 magnifies the amplitude of dominant mode by 11 dB while the Strouhal number reduces. Figure 9(b) presents the spectrum of cases which oscillate in the wake mode. It is observed that the Strouhal number of the dominant mode for all cases almost equals to 0.26. It can be deduced that the frequency of oscillation in terms of Strouhal number is independent of Mach number. Thus, the acoustic-feedback coupling is absent for wake mode. Furthermore, the rate of amplification of fluctuations due to variation of Mach number in wake mode is smaller than that of the shear-layer mode.

In order to evaluate the performance of URANS, oscillation characteristics (i.e. frequency and amplitude) need to be compared to higher order methods. The frequencies of the most dominant peak in the spectra for all simulations, as well as predictions from Rossiter's model (Rossiter 1964), LES (Rubio, De Roeck, Baelmans, and Desmet, 2007) and DNS (Rowley, 2002) are presented versus Mach number in Fig. 10. The results of URANS computations coincide DNS solutions except the case $M=0.2$ where it overestimates both DNS and LES predictions. It should be pointed out that the shear-layer mode flow oscillation of cases $M=0.2$ and $M=0.3$ have fluctuation frequencies which meet the second Rossiter's mode. For the cases which oscillate in wake mode, i.e. $M=0.4$ to 0.7 , the dimensionless frequency does not change with the variation of free stream Mach number. Regarding

the flow oscillation amplitude, the only available data in literature is power spectral density of velocity for LES simulations (Rubio, De Roeck, Baelmans, and Desmet, 2007). Figure 11 shows the power spectral density of velocity for LES (11.a) (cfr (Rubio, De Roeck, Baelmans, and Desmet, 2007)) along with their URANS counterpart (11.b). Comparison of the amplitudes for the first dominant mode indicates an excellent agreement between the two set of results.



(a) M=0.4 to 0.7



(b) M=0.2 to 0.3

Fig. 9. Power spectra of pressure at the point located on top of the cavity.

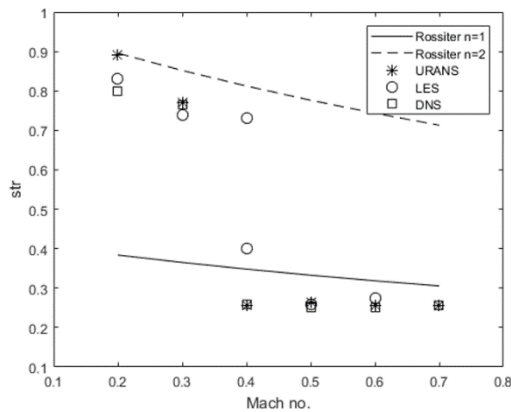
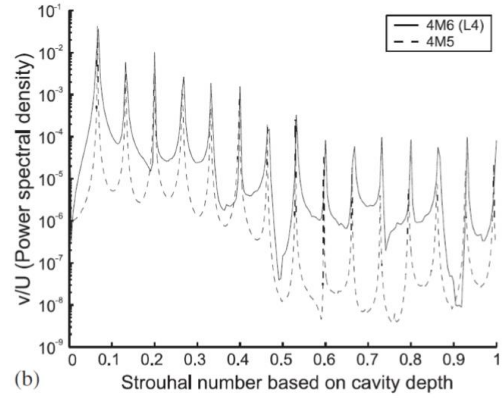
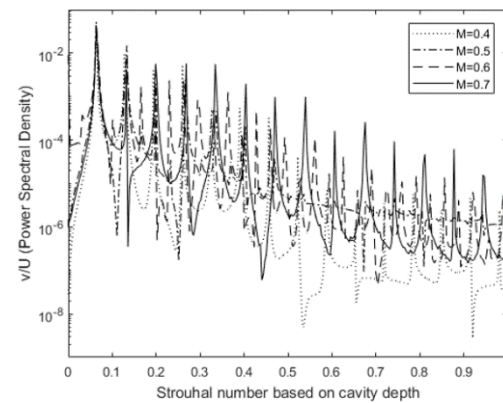


Fig. 10. Strouhal numbers for peaks in spectra compared to Rossiter's model.



(a) LES results of (Rubio, De Roeck, Baelmans, and Desmet 2007)



(b) URANS results

Fig. 11. Power spectral density of $\frac{v}{U_\infty}$.

5. SUMMARY AND CONCLUSIONS

The present work aims to evaluate the performance of RANS/URANS as a basis of a hybrid approach to capture the tonal noise. For this purpose, the Reynolds-averaged Navier-Stokes equations were solved to identify the flow-induced oscillation modes in a shallow cavity. The transition SST $k - \omega$ model was implemented to perform the two dimensional flow simulations. The cavity has a length to depth ratio of 4 and computations are carried out for flow with a constant Reynolds number of 1500 and its Mach number ranging from 0.2 to 0.7.

The solutions of URANS reveal two modes of oscillations: shear-layer mode and wake mode. In the shear-layer mode, observed in cases with a free stream Mach number of 0.2 and 0.3, propagation of scattered acoustic waves at the trailing edge and receptivity of the shear-layer to them at leading edge results in oscillations at the Rossiter frequencies. In the wake mode, realized for the cases M=0.4 to 0.7, oscillation frequencies are independent of Mach number. The modes identified by URANS are similar to the DNS results available in literature except for M=0.3, where DNS detects a mixed mode. It should be remarked that only one flow oscillation mode is discerned for each case by the URANS

computations. Time averaged URANS solutions are compared to their RANS counterpart for shear-layer mode and wake mode oscillations. It is shown that the flow patterns specifically for the wake mode drastically change. Therefore, the steady RANS solution can not truly represent the flow features since the impact of unsteadiness is not negligible. In these circumstances, steady RANS solution is not suitable to be coupled with SNGR method. Regarding the predicted oscillation's frequencies and amplitude, an excellent agreement is observed between URANS and other higher order methodologies, i.e. DNS and LES, in the wake mode. In the shear layer mode, the dominant frequency compares well with that obtained via Rossiter's formula and slightly overestimates the DNS and LES predictions.

The major conclusion based on the presented works is that the URANS approach is a reliable tool for identification of different oscillation regimes and is thus capable of providing information for further acoustic computations.

ACKNOWLEDGEMENT

This work was supported by Shahid Beheshti University, GC., under contract number 600/1504 and also the computational resources are provided by the Center for High Performance Computing (SARMAD) of the university which are gratefully acknowledged.

REFERENCES

Ahn, H., F. S. Lien, J. Larsson and J. Hines (2008). Simulation of aeroacoustic resonance in a deep cavity with grazing flow using a pressure-based solver. *International Journal of Computational Fluid Dynamics* 22(1-2), 39-47.

Ali, I., S. Becker, J. Utzmann and C. Munz (2008). Aeroacoustic study of a forward facing step using linearized Euler equations. *Physica D: Nonlinear Phenomena* 237(14), 2184-2189.

Ashcroft, G., K. Takeda and X. Zhang (2003). A numerical investigation of the noise radiated by a turbulent flow over a cavity. *Journal of Sound and Vibration* 265(1), 43-60.

Chang, K., G. Constantinescu and S. Park (2006). Analysis of the flow and mass transfer processes for the incompressible flow past an open cavity with a laminar and a fully turbulent incoming boundary layer. *Journal of Fluid Mechanics* 561, 113-145.

De Roeck, W., G. Rubio, M. Baelmans and W. Desmet (2009). Toward accurate hybrid prediction techniques for cavity flow noise applications. *International journal for numerical methods in fluids* 61(12), 1363-1387.

Djambazov, G., C. H. Lai and K. Pericleous (2000). On the coupling of navier-stokes and linearised Euler equations for aeroacoustic simulation.

Computing and visualization in science 3(1), 9-12.

Gharib, M. and A. Roshko (1987). The effect of flow oscillations on cavity drag. *Journal of Fluid Mechanics* 177, 501-530.

Gloerfelt, X., C. Bogey and C. Bailly (2002). LES of the noise radiated by a flow over a rectangular cavity. *7th AIAA/CEAS Aeronautics Conference*, 7-8.

Henderson, J., K. Badcock and B. Richards (2000). Subsonic and transonic transitional cavity flows. *6th Aeroacoustics Conference and Exhibit*, 1966.

Kutlu, B., B. Saracoglu, G. Paniagua and J. Kapat (2015). Aeroacoustics of flow over rectangular cavities. *51st AIAA/SAE/ASEE Joint Propulsion Conference*, 3929.

Larchevêque, L., P. Sagaut, T. H. Le and P. Comte (2004). Large-eddy simulation of a compressible flow in a three-dimensional open cavity at high Reynolds number. *Journal of Fluid Mechanics* 516, 265-301.

Li, W., T. Nonomura and K. Fujii (2013). On the feedback mechanism in supersonic cavity flows. *Physics of Fluids* 25(5), 056101.

Li, W., T. Nonomura, A. Oyama and K. Fujii (2012). Feedback mechanism in supersonic laminar cavity flows. *AIAA journal* 51(1), 253-257.

Lucas, J. M., O. Cadot, V. Herbert, S. Parpais, and J. Détery (2017). A numerical investigation of the asymmetric wake mode of a squareback ahmed body—effect of a base cavity. *Journal of Fluid Mechanics* 831, 675-697.

Maillard, D. and C. Bailly (2001). Numerical simulation of the unsteady flow past a cavity and application to the sunroof buffeting. *ERCOFTAC Workshop on LES for Acoustics*.

Menter, F., R. Langtry, S. Likki, Y. Suzen, P. Huang and S. Völker (2006). A correlation-based transition model using local variables- part i - model formulation. *Journal of turbomachinery* 128(3), 413-422.

Mesbah, M. (2006). *Flow noise prediction using the stochastic noise generation and radiation approach*. PhD Thesis, Katholieke Universiteit Leuven.

Mesbah, M., J. Meyers and M. Baelmans (2008). Acoustic performance of nonreflecting boundary conditions for a range of incident angles. *Journal of Computational Acoustics* 16(01), 11-29.

Nair, K. and S. Sarkar (2017). Large eddy simulation of self-sustained cavity oscillation for subsonic and supersonic flows. *Journal of Fluids Engineering* 139(1), 011102.

Rossiter, J. (1964). *Wind tunnel experiments on the flow over rectangular cavities at subsonic and transonic speeds*. Technical report, Ministry of

- Aviation; Royal Aircraft Establishment; RAE Farnborough.
- Rowley, C. (2002). *Modeling, simulation, and control of cavity flow oscillations*. Ph.D. thesis, California Institute of Technology.
- Rubio, G., W. De Roeck, M. Baelmans and W. Desmet (2007). Numerical identification of flow-induced oscillation modes in rectangular cavities using large eddy simulation. *International journal for numerical methods in fluids* 53(5), 851-866.
- Shao, W. and J. Li (2015). Analytical and numerical investigations on the aeroacoustical oscillation of flow past the cavity. *ASME Turbo Expo 2015: Turbine Technical Conference and Exposition*, V02BT41A005–V02BT41A005.
- Shieh, C. and P. Morris (2001). Comparison of two- and three-dimensional turbulent cavity flows. *AIAA paper* 511, 2001.
- Shih, T. H. and N. S. Liu (2004). From RANS towards LES for engine turbulent flows. 42nd *AIAA Aerospace Sciences Meeting and Exhibit*, 160.
- Sinha, N., S. Dash, N. Chidambaram and D. Findlay (1998). A perspective on the simulation of cavity aeroacoustics. *AIAA paper* (98-0286).
- Sun, Y., K. Taira, L. N. Cattafesta and L. S. Ukeiley (2017). Spanwise effects on instabilities of compressible flow over a long rectangular cavity. *Theoretical and Computational Fluid Dynamics* 31(5-6), 555-565.
- Sun, Y., Q. Liu, L. N. Cattafesta III, L. S. Ukeiley, and K. Taira (2018). Effects of side-walls and leading-edge blowing on flows over long rectangular cavities. *AIAA Journal* 57(1), 106-119.
- Wang, H., M. Sun, N. Qin, H. Wu and Z. Wang (2013). Characteristics of oscillations in supersonic open cavity flows. *Flow, turbulence and combustion* 90(1), 121-142.